RSC Advances

PAPER

View Article Online
View Journal | View Issue

Cite this: *RSC Adv.*, 2022, **12**, 34006

Treatment of fluorinated wastewater with chitosan modified activated sludge lysis ash

Xiangdong Li,[a] Yanwen Guo,*[a] Yuhan Xie[a] and Yue Sun[b]

Received 26th August 2022
Accepted 17th November 2022

DOI: 10.1039/d2ra05343h

rsc.li/rsc-advances

Preparation of a novel environmentally friendly and cost-effective composite adsorbent for fluoride removal is presented in this work. An activated sludge lysis ash/chitosan (ASLA/C) composite adsorbent was synthesised using an *in situ* coprecipitation method, and the removal effect of the material was analysed by static adsorption, isothermal adsorption and kinetic adsorption tests. Langmuir model could better describe the adsorption process and the adsorption was in accordance with the kinetic equation of the pseudo-second-order kinetics reaction. The values of adsorption thermodynamic and kinetic parameters were indicated that the adsorption of fluoride ions is a spontaneous, heat-absorbing entropic process, and the reaction was carried out by a combination of mechanisms, such as electrostatic adsorption, ion exchange, surface complexation and hydrogen bonding. The experimental results indicated that ASLA/C can be used as a cheap and readily available alternative efficient adsorbent where the maximum fluorinate absorption was observed with 7.714 mg g^{-1}, while solving the problem of waste from activated sludge lysis disposal and realizing the environmental benefits of waste.

1. Introduction

Fluorine is a trace element necessary for human life activities, dental health, bone growth and development; however, long-term exposure to fluorine-rich drinking water can cause health hazards in people.[1] A concentration of fluoride ions in drinking water greater than 1.5 mg L^{-1} will have a serious impact on human health. In areas with severe fluoride ion contamination, chronic diseases such as dental fluorosis and bone fluorosis occur in large numbers, endangering human health. Endemic fluorosis is a worldwide environmental and geological problem that seriously endangers human health and has caused widespread concern worldwide.[2] The efficiency of fluoride removal by adsorption is mainly dependent on the performance of the adsorbent materials, which can be classified according to their raw material components as natural and modified polymer adsorbents, rare earth adsorbents and modified metal oxide adsorbents.[3,4] Based on this, this paper focuses on the study of organically modified industrial waste residue composite adsorbent materials.

Industrial and agricultural wastes are byproducts of industrial and agricultural production and processing in large quantities. If these wastes are used as adsorbents, it not only does reduce production costs, but also reduces the environmental pressure caused by the waste treatment and disposal process and allows the waste to be reused, thus achieving the goal of treating waste with waste. Industrial and agricultural waste is now widely used for the removal of heavy metals, dyes and other pollutants from water.[5,6] Studies have verified that straw ash,[7] electrocoagulated (EC) sludge,[8] modified clay composite materials,[9] high-temperature modified eggshells,[10] and crushed clay pots[11] show promise in fluoride removal. Meanwhile, activated sludge also can be used as a good adsorption material with the advantages of low price, high efficiency, good selectivity, and a wide applicability range of pH and temperature,[12,13] but there is a lack of reported studies related to the use of activated sludge lysis ash as a fluoride adsorption material.

Lysis has become a new method of disposal for industrial and agricultural waste, Ako reported on the use of Advanced Kinetics and Technology Solutions (AKTS) thermodynamic software to simulate and calculate the activation energy (E_a) and other kinetic parameters of the remaining solid digestate, the work highlights that the potential for solid waste cracking for disposal.[14,15] But the process will inevitably produce large amounts of ash, which will create new disposal problems.[16] The large quantities of sludge generated as waste from treatment plants and the residues from their subsequent lysis process remain environmental issues. In recent research, Ahmed used low-value lignocellulosic materials to synthesize activated carbon into value-added products offers new ideas for a circular economy.[17] Emerging research therefore requires the sustainable treatment of sludge lysis ashes as a value-added resource. For example, their conversion into high value-added products such as sorbents is a favourable route to resource utilisation

[a]*School of Environment Science and Spatial Informatics, China University of Mining and Technology, Xuzhou 221116, China. E-mail: guoyw0987@gmail.com*
[b]*Jiangsu Vocational Institute of Architectural Technology, No. 26 Xueyuan Road, Xuzhou 221433, China*

and secondary pollution control, as they are an unused resource that also presents serious disposal problems. The preparation of sorbents from lysis ash is a cost-effective alternative adsorbent that is of interest in the fields of material recovery, resource utilisation and industrial wastewater treatment. Therefore, the use of recovered sludge lysis ash for the preparation of composite adsorbents can serve the dual purpose of resource utilisation and environmental management.

Chitosan (a copolymer of 2-glucosamine and *N*-acetyl-2-glucosamine) is mainly derived from crustaceans such as shrimp, crabs and lobster and is a nontoxic, biodegradable and biocompatible material. Studies have shown that chitosan-modified adsorbents have good treatment effects.[18,19] The chitosan molecular chain contains a large number of amino groups, which can easily undergo protonation under acidic conditions, making it ligated with metal ions to form chelates and play a role in the adsorption of metal ions, while there are a large number of hydroxyl groups on its branched chain, which also have a certain adsorption effect on fluorine ions.[20,21]

There are few reports on the use of activated sludge lysis ash in combination with chitosan for the adsorption of fluoride in solution. In this study, chitosan was used to modify activated sludge lysis ash to investigate its ability to remove fluoride from water, and its removal effect and adsorption mechanism were explored. Chemical modification enables the synthesis of composites with porous structures while yielding materials with higher surface areas. Ahmed *et al.* prepared high surface area (1368 $m^2 g^{-1}$) cracked materials from manzanita lignocellulose using NaOH activation modification.[22] Kong *et al.* synthesized novel nanostructured lanthanide-doped hydrotalcite composites La@MgAl by hydrothermal calcination and prepared surface area of 123.28 $m^2 g^{-1}$ and showed good results in the removal of fluorinated wastewater.[23] The modified neem husk lysis material prepared from potassium hydroxide activated Jatropha wood by Alau *et al.* had a high specific surface area of 1305 $m^2 g^{-1}$.[24] Thus, in terms of porosity and surface area, the chemical modification showed a better adsorption potential.

In this study, a new material was prepared for the removal of fluoride ions from wastewater through the recycling of activated sludge lysis ash modified by chitosan. In addition, the effects of the adsorbent dose, solution pH, different initial fluoride concentrations, and reaction time on the adsorption capacity were also investigated. The aim is to confirm the use of activated sludge lysis ash as an inexpensive and readily available adsorbent material in the treatment of fluorinated wastewater. To provide new ideas for the disposal of solid waste and to provide theoretical support for its commercial-scale application.

2. Materials and methods

2.1. Materials and reagents

The treatment material used in this experiment was obtained from the product of the remaining sludge pyrolysis ash were collected from Kai Li factory, China, Guizhou wastewater treatment plant. It was sieved and processed to control the particle size range between 0.6 and 1.2 mm, washed with deionized water and then dried in an oven at 80 °C for 24 hours. After adding quantitative chitosan to acetic acid with a mass fraction of 2% (wt) and dissolving magnetically at room temperature to form a transparent solution, quantitative activated sludge lysis ash was added and reacted with magnetic stirring for 2 h and left for 48 h, and then, the activated sludge lysis ash/chitosan (ASLA/C) composite adsorbent was obtained after extraction, washing and drying (the process is shown in Fig. 1).

All chemical reagents used in this work were analytically pure (A. R.), and chitosan with a deacetylation degree ≥95% and viscosity of 100–200 MPa s from MACKLIN was used, while NaF solution was prepared manually as simulated high-fluorine water. NaF powder was dried at 103–110 °C for 2 h, and a standard stock solution of 20 mg per L NaF was prepared for subsequent batch experiments.

2.2. Characterization methods

The adsorbent morphology of ASLA and ASLA/C was observed using scanning electron microscopy (SEM) (Inspect™ Inspect F50) at various magnifications. The phase of the adsorbent was investigated using X-ray diffractions (XRD) (Shimadzu, MAXima-X XRD-7000). Experiments were carried out using CuK radiation at 40.0 kV and the continuous scanning range of the

Fig. 1 Preparation process of activated sludge lysis ash/chitosan (ASLA/C).

instrument was 10–70°. The N_2 adsorption–desorption isotherms of the samples at liquid nitrogen temperature (77 K) were determined using an ASAP 2000 automatic physical adsorption instrument (Mack, USA), the specific surface area of the products was calculated using the BET equation, and the pore size pore volume distribution of the products was calculated using the BJH method. The infrared spectrum was recorded on a Nicolet Nexus 670 Fourier infrared transform (FTIR) spectrophotometer at a wavelength range from 400–4000 cm^{-1}.

2.3. Batch experiments

2.3.1. Chitosan content proportioning experiments. The material ratios were mainly for the ratios between chitosan and activated sludge lysis ash (ASLA), where chitosan was added at 0 g, 0.2 g, 0.4 g, 0.6 g, 0.8 g and 1.0 g, and ASLA was added at a fixed amount of 1.0 g. The preparation process will be carried out according to the steps in Section 2.1, and the best material ratios were obtained according to experimental optimization.

2.3.2. Fluoride ion adsorption experiments. One hundred millilitres of a certain concentration of fluoride ion solution was placed in a conical flask, the ASLA/C adsorbent was added, the pH was adjusted with 0.1 mol L^{-1} hydrochloric acid and sodium hydroxide, and the reaction was performed at room temperature (20 °C). The supernatant was passed through a 0.45 μm filter membrane after 30 minutes of standing, and the concentration of fluoride ions in the reaction solution was determined using a fluoride ion electrode. In batch adsorption experiments, the effects of initial fluorine concentration (1, 2, 4, 6, 10 and 20 mg L^{-1}), reaction time (10–340 min), solution pH (2–11) and the amount of adsorbent (0.1, 0.3, 0.5, 0.7, 0.9, 1.0 and 1.1 g/100 mL) were separately considered. The amount of fluorine adsorbed and the fluoride removal rate were calculated as follows:

$$Q = \frac{(C_0 - C_e)V}{M} \quad (1)$$

$$R = \frac{(C_0 - C_e)}{C_0} \times 100\% \quad (2)$$

where Q is the adsorption capacity at adsorption equilibrium (mg g^{-1}); C_0 is the initial concentration of F^- in the solution (mg g^{-1}); C_e is the residual concentration of F^- in the solution at adsorption equilibrium (mg g^{-1}); V is the volume of the solution (mL); M is the mass of dry matter of the adsorbent material added (g); and R is the removal rate of F^-.

3. Results and discussion

3.1. Effect of chitosan content

To five beakers, 100 mL of simulated wastewater (C_0 = 10 mg L^{-1}), 1.0 g of pure ASLA, and 0.2–1.0 g of chitosan were added as described above. The reaction time was set at 180 min, and the pH = 5. The reaction was left to stand after completion for 30 min, and the relationship curve between the loading of chitosan and the removal effect was obtained, as shown in Fig. 2. The fluoride removal efficiency was only 0.043 mg g^{-1} without chitosan, and the fluoride removal efficiency increased from 30.26% to 84.78%. This is mainly because the surface of chitosan is positively charged, and the compound with ASLA increases the positive charge on the surface of the adsorbent, which improves the binding capacity of fluoride ions and therefore the efficiency of fluoride removal.[24] Meanwhile, the large number of $-NH_2$ and –OH groups in chitosan, which are naturally powerful in adsorption, help to produce NH_F groups. Therefore, chitosan occupies a larger proportion in the mass ratio of composite adsorbents. When the chitosan content added to the composite adsorbent was increased from 0.2 g to 0.8 g, and then gradually decreased as the chitosan content increased. The optimum fluoride removal efficiency was 84.78% for ASLA/C with a mass ratio of chitosan to ASLA of 4 : 5 and an adsorption capacity of 1.69 mg g^{-1}. Subsequent studies were carried out on the basis of ASLA modified by 0.8 g of chitosan with coprecipitation.

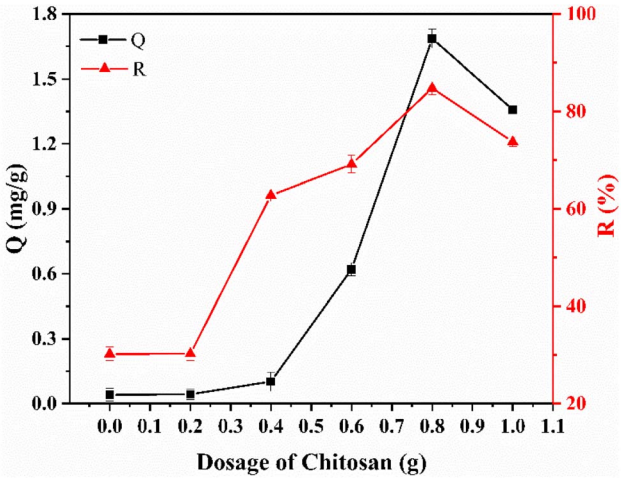

Fig. 2 Effect of chitosan dose on the fluoride removal effect of ASLA/C. Adsorption conditions: C_0 = 10 mg L^{-1}, pH = 5, m = 1.0 g, t = 180 min, T = 20 °C.

ASLA itself has moderate mechanical strength and granularity, and in a reaction with chitosan modified composite adsorbent, the mechanical strength and surface properties of the adsorbent are improved with adsorption. The appropriate proportion of chitosan in the composite adsorbent helps to ensure the mechanical strength of the adsorbent and makes it easy to shape and form particles, which can be used for static or dynamic fluoride removal.

3.2. Characterization of the adsorbents

3.2.1. Diffraction pattern analysis. A distinct diffraction peak appears in the XRD pattern at a 2θ of approximately 32°, and $CaMg(CO_3)_2$ (dolomite) and SiO_2 (quartz) are the main composition of ASLA. Kaolinite ($Al_2(Si_2O_5)(OH)_4$), another component of lysis ash, has a crystal structure consisting of a 1 : 1 lamellar structure formed by the arrangement of silicon–oxygen tetrahedral sheets and aluminum–oxygen octahedral sheets, which have a large specific surface area and pores between layers, exhibiting a high adsorption capacity for heavy metals.[25] After compounding with chitosan, the position of the

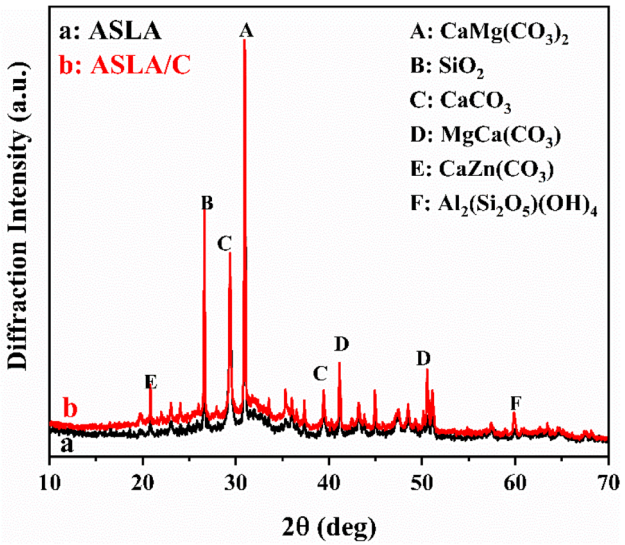

Fig. 3 XRD patterns of ASLA and ASLA/C.

characteristic absorption peak basically did not change, while the intensity of the absorption peak was enhanced (Fig. 3). This indicates that the crystalline shape of dolomite does not change after compounding with chitosan, but only the crystallinity increases.[26]

The oxide and elemental content of ASLA were determined using XRF (Table 1), and the main oxides were SiO_2, Al_2O_3, CaO and Fe_2O_3, which were similar to the XRD test results, further demonstrating that the main elements of the sludge lysis ash composition were Si, Ca, O, Al and Fe. The main components of the modified ASLA/C were found to be unchanged, but the percentage contents were increased. This is probably because the chitosan used in the preparation of ASLA/C provided aluminium, which was loaded on ASLA in the form of an activator, while other elements were also introduced in small amounts.

3.2.2. Surface morphology analysis. The surface morphology of ASLA and ASLA/C was observed by SEM, as shown in Fig. 4. Under 5.0k magnification, the surface of ASLA was flat and smooth with no obvious porous structure. However, after modification, ASLA/C has a large number of flocculent and agglomerated structures, and the roughness of its surface increased, probably due to the formation of new pores and surfaces by mutual lap and winding between chitosan molecules. In general, the rough surface structure will provide a larger specific surface area than the blocky and smooth surface structure, which is favour for the adsorption of fluorine ions and the occurrence of chemical complexation. The composite was prepared mainly by coprecipitation and SEM images further confirmed that chitosan was interspersed in ASLA. The exchange of fluorine ions occurs mainly on the surface of ASLA, and the increase in adsorption capacity depends mainly on the grain size and specific surface area. If chitosan coalesces excessively on the surface of ASLA, the specific surface area is reduced and the adsorption capacity is lowered. It was therefore confirmed that when the chitosan content was further increased, the excess chitosan clogged the pores of the ash, resulting in a reduction in fluoride removal efficiency.[27]

The N_2 adsorption–desorption curves and pore size distribution curves of the ASLA and ASLA/C samples are shown in Fig. 5. There are six recognized isotherm types, and according to the IUPAC classification, the ASLA samples showed obvious type IV isotherms at relative pressures 0.5–1.0 with H3 hysteresis loops, and the samples of ASLA/C showed a sharp increase in N_2 adsorption at higher relative pressures 0.8–1.0, indicating that

Table 1 Composition analysis of (a) ASLA and (b) ASLA/C by XRF

Composite	SiO_2	Al_2O_3	CaO	Fe_2O_3	P_2O_5	MgO	SO_3	K_2O	TiO_2	Na_2O
ASLA	8.18	11.3	33.24	6.52	5.43	3.25	2.95	0.36	0.23	0.14
ASLA/C	12.42	22.87	32.35	12.22	8.92	5.88	2.69	0.58	0.51	0.29

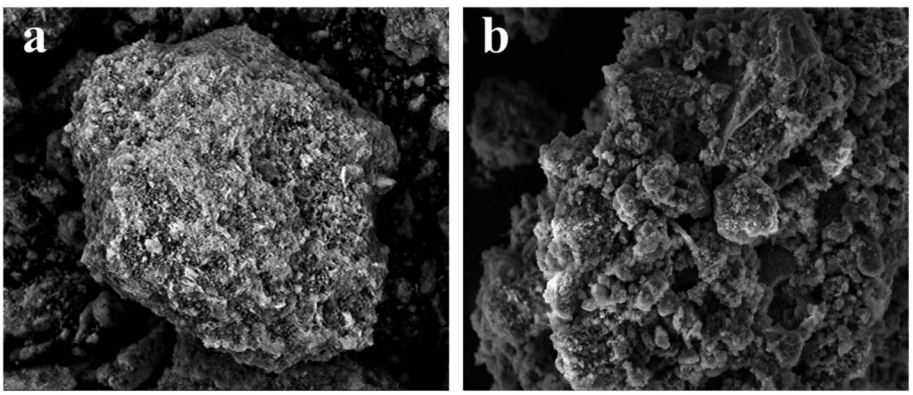

Fig. 4 Scanning electron microscopy images of (a)ASLA and (b) ASLA/C.

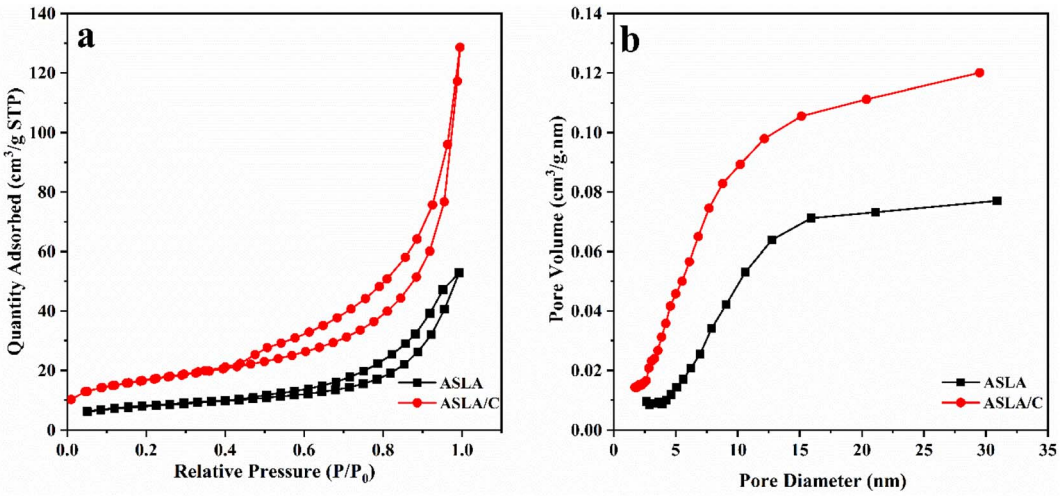

Fig. 5 (a) N_2 adsorption–desorption isotherms and (b) pore size distribution of ASLA and ASLA/C.

the modified materials have irregular mesoporous structures and that some slit pore structures formed by the accumulation of lamellar particles. The BET surface area and pore volume of ASLA/C were significantly higher than those of ASLA, indicating that modification with chitosan could improve the pore structure properties and enhance the N_2 molecule trapping ability. ASLA/C has a richer pore structure and larger specific surface area than before, and its specific surface area was 57.46 $m^2\ g^{-1}$, which is approximately twice that of ASLA (26.91 $m^2\ g^{-1}$). The total pore volume of ASLA/C was 0.113 $cm^3\ g^{-1}$ and that of ASLA was 0.081 $cm^3\ g^{-1}$, indicating that the specific surface area and pore volume of ASLA were effectively increased after chitosan modification, and more active sites were provided. The average pore size determined by the BJH model analysis of ASLA/C was 16.5 nm, and the average pore size increased accordingly after chitosan modification.

3.2.3. Functional group determination. Fig. 6 shows that the same characteristic peaks exist at approximately 3371.93, 1428.99, 1042.82, 875.52 and 566.49 cm^{-1} for the material before and after modification. The broad peak near 3371 cm^{-1} is mainly the OH stretching vibration peak, ν_{OH} (containing water and organic OH functional groups); the peak near 2928 cm^{-1} is mainly the CH stretching vibration peak, ν_{CH}; the peak near 2520 cm^{-1} is mainly the sum frequency peak of the symmetric and antisymmetric stretching vibration peak of carbonate (calcite, dolomite), $\nu_{as\ CO_3} + \nu_{s\ CO_3}$. The peak near 1640 cm^{-1} is mainly the in-plane bending vibration peak of OH, δ_{OH}; the nearby peak at 1428 cm^{-1} is mainly the stretching vibration peak of carbonate (calcite, dolomite), $\nu_{as\ CO_3}$; the peak at 1042 cm^{-1} is mainly the stretching vibration peak of Si–O bonds in some silicon–aluminates (containing structures such as Si–O–Si and Si–O–Al) (the symmetric stretching vibration peak of carbonate is near 1080, which may be masked, and the antisymmetric stretching vibration peak of phosphate is also near 1040). ν_{Si-O}; the out-of-plane bending vibration peak of carbonate, γ_{CO_3}, is predominant near 876 cm^{-1}; the bimodal

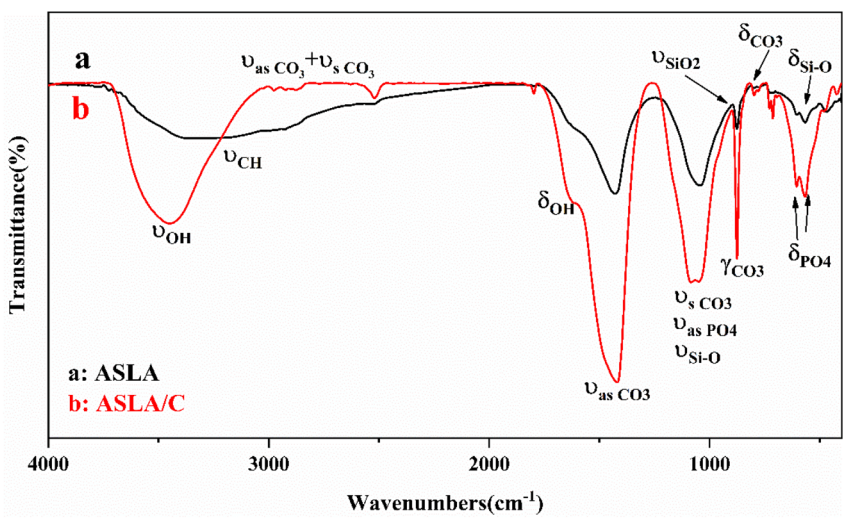

Fig. 6 FTIR characterization of ASLA and ASLA/C.

structure near 799 and 777 cm^{-1} is typical of the Si–O stretching vibration peak of quartz, $\nu_{Si-O,}$ and the in-plane bending vibration peak of carbonate, δ_{CO_3} is predominant near 726 cm^{-1}; the peak near 604 and 567 cm^{-1} may be the bending vibration peak of phosphate, δ_{PO_4};and the peak near 468 cm^{-1} is mainly the bending vibration peak of some Si–O bonds δ_{Si-O} (containing Si–O–Si, Si–O–Al, Si–O–Mg, and Si–O–Fe structures).[28] These oxygen-containing functional groups are electron-absorbing groups, which strengthen the electrostatic attraction of activated carbon and facilitate the adsorption process. Compared with that before modification, the position of the characteristic absorption peaks basically did not change but was enhanced. This indicates that the crystal structure of the adsorbent was not affected after chitosan compounding, while the crystallinity increased. The results are consistent with the XRD results.

3.3. Batch adsorption experiments

3.3.1. Effect of reaction time. In this experiment, the reactions were carried out in solutions with a dose of ASLA/C of 1.0 g, pH = 5 and an initial concentration of F^- of 10 mg L^{-1} for 10, 20, 30, 40, 50, 60, 90, 120, 150, 180, 220, 260, 300 and 340 min at 20 °C. The results are shown in Fig. 7(a). As the adsorption time increases, the adsorption volume Q rises sharply and then rises slowly to a plateau, and the instantaneous adsorption rate (dQ/dt) decreases gradually. The curve can be divided into three segments: the first period (adsorption time <60 min) has a large slope, and the adsorption volume rises sharply, with approximately 55% of the total adsorption volume completed within 60 min, indicating that adsorption at this stage is a rapid adsorption process. The slope of the second period (60–250 min) is smaller, with a slow increase in adsorption over time, with approximately 35% of the total adsorption completed in this period, probably due to the full use of the active site on the adsorbent or physical adsorption.[29] The third stage (adsorption time >250 min) is a plateau where adsorption reaches equilibrium and the amount of adsorption does not increase with time. Therefore, the adsorption of fluoride by ASLA/C is a fast adsorption process, which achieved equilibrium within 250 min.

3.3.2. Effect of adsorbent dose. Dose is an important parameter that determines the adsorption capacity of the adsorbent. To determine the appropriate dose, the adsorption of 10 mg L^{-1} fluoride solutions (100 mL) by ASLA/C at pH = 5 for 250 min was studied at doses of 0.1, 0.3, 0.5, 0.7, 0.9, 1, 1.1 and 1.3 g. Fig. 7(b) shows the effect of ASLA/C dosing on the effect of fluoride treatment at 20 °C. As seen from the figure, the fluoride adsorption capacity of ASLA/C increased from 0.83 mg g^{-1} to 1.04 mg g^{-1} and 1.49 mg g^{-1} when the adsorbent dose was increased from 0.1 g to 0.5 g and 1.0 g in solution, and the removal rate of fluorine ions increased from 57.82% to 66.08% and 89.13%. The highest removal rate of F^- in the range of adsorbents studied was achieved when the amount of adsorbent reached 1.0 g. This is mainly because as the amount of

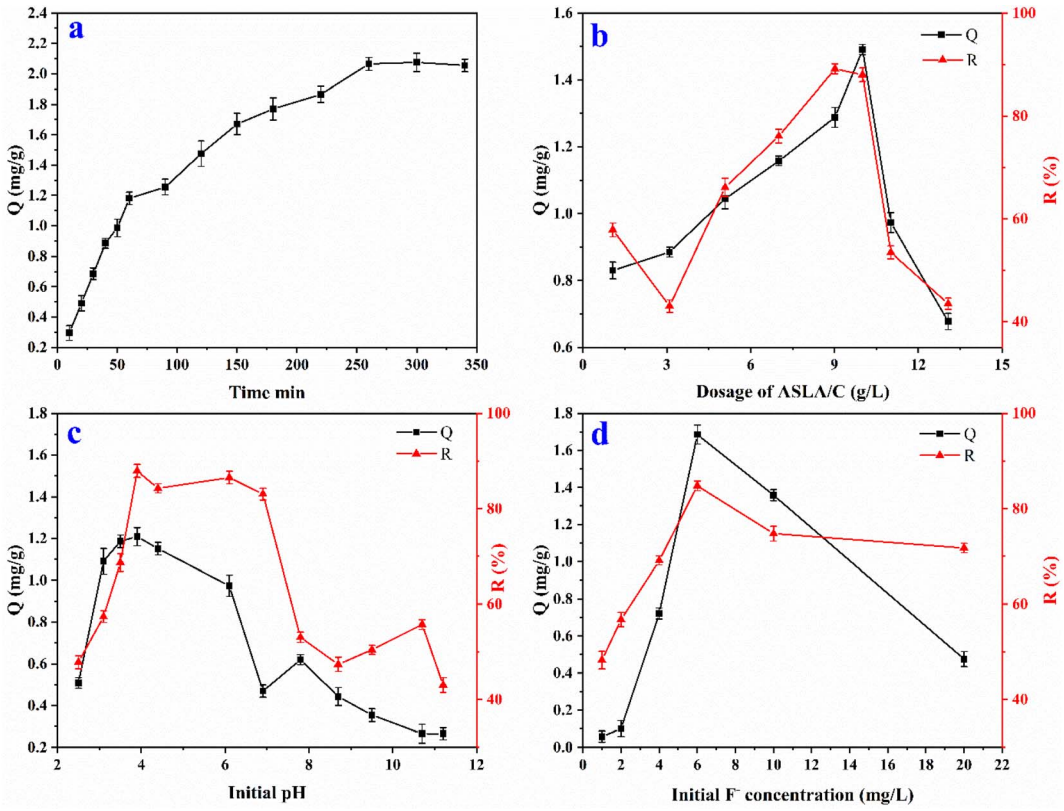

Fig. 7 Effect of (a) reaction time; (b) adsorbent dose; (c) solution pH and (d) initial F^- concentration on the fluoride adsorption capacity and removal capacity.

adsorbent increases, the adsorption sites available on the surface of the adsorbent also gradually increase, and therefore the removal rate gradually increases. The increase in the amount of adsorbent added to the reaction provided more adsorption sites for fluoride removal. Combined with the BET analysis, the large specific surface area of ASLA/C further increased the binding sites and facilitated the removal of fluoride. As the initial fluorine solution concentration remained constant, the change in fluorine removal rate continued to decrease to 43.48%, even after continuing to increase the amount of adsorbent. This may be due to the saturation of the adsorption, combined with the large number of ASLA particles squeezing each other, resulting in a decrease in specific surface area and pore volume.[30] In summary, 10 g L^{-1} was chosen as the optimum dose for the subsequent study.

3.3.3. Effect of initial pH. To investigate the effect of different initial pH values on the adsorption effect, the pH of the 10 mg L^{-1} fluoride solution was adjusted to 2, 3, 4, 5, 6, 7, 8, 9, 10 and 11, the experiment lasted 250 min at 20 °C and the effect of 1 g of ASLA/C on the removal of F^- was determined as shown in Fig. 7(c). The fluorine adsorption capacity and fluorine removal rate of fluorine by ASLA/C decreased significantly with pH over 6 of the solution, and the acidic environment with a pH of 4–6 was more favourable for the removal of fluoride. The adsorption capacity of ASLA/C was continuously and steadily increasing from pH 4 to 6, and the removal rate increased from 47.82% to 86.52%. This is because the surface of the material is positively charged by the formation of $-OH_2^+$ and F^- can be adsorbed onto the surface of the material through electrostatic attraction. The acid dissociation constant of HF is 3.2, and at pH < 3.2 fluorine is mainly in the HF form (the adsorbent is unable to adsorb F^- in the HF state), resulting in few free fluoride ions being adsorbed by the adsorbent, resulting in low removal rates and adsorption volumes.[31,32] As the pH gradually increases, the OH^- content in the solution increases, and the amount of active binding sites on the surface of the adsorbent decreases, resulting in a faster decrease in the adsorption effect. When pH > 7, the ASLA/C surface becomes negatively charged, which prevents the adsorption of anions. At the same time, OH^- competes with F^- for adsorption and the probability of contact between F^- and the adsorption site, resulting in a significant reduction in adsorption and removal rates.[33] In addition, when the initial pH of the solution is greater than 9, the reaction system contains a large amount of negative charges and the surface of the adsorbent material has fewer binding active sites,[34] which has a homogeneous charge repulsion effect with the equally negatively charged fluoride ions. Therefore, the electrostatic repulsion is also an important factor in the significant decrease in the adsorption efficiency of fluorine ions by ASLA/C under alkaline conditions. Compared to fluoride ions, hydroxide has a stronger affinity to the surface of ASLA/C; at pH 11, and the fluorine adsorption capacity and fluorine removal rate of ASLA/C were only 0.67 mg g^{-1} and 42.71%, respectively.

3.3.4. Effect of initial fluoride concentration. The fluoride removal effect at different concentrations of solutions (1, 2, 4, 6, 10 and 20 mg L^{-1}) was investigated by adding 1.0 g of composite adsorbent at pH = 4 and 20 °C for 250 min. As shown in Fig. 7(d), the initial concentration of fluoride ions in the solution increased continuously within a certain range, and the adsorption amount increased continuously from 0.058 mg g^{-1} to 1.69 mg g^{-1}. After the concentration of the solution exceeded 6 mg L^{-1}, the adsorption amount of F^- no longer increased with the concentration of the solution. The fluoride removal decreased from 84.78% to 71.73%, while the adsorption capacity decreased to 0.47 mg g^{-1}. This is mainly because when the amount of adsorbent is constant, its maximum adsorption capacity is also fixed. When the initial concentration of the solution is low, fluoride is more easily adsorbed on the adsorbent surface, and the adsorption sites of the adsorbent are not saturated at this time.[35] Although the initial fluoride ion concentration gradually increased, when a certain amount of ASLA/C adsorption sites reached saturation, the excess fluoride could not be continued, so when the initial fluoride ion concentration in solution exceeded the ASLA/C adsorption saturation capacity, the fluoride ion removal rate gradually decreased.

3.4. Adsorption kinetics

To further investigate the adsorption mechanism of ASLA/C as an adsorbent for fluoride, pseudo-first-order, pseudo-second-order and intraparticle diffusion reaction models were used to fit the adsorption kinetic processes.[36–38] The pseudo-first-order model assumes that the adsorption process depends on the solution concentration and effective adsorption sites, while the pseudo-second-order kinetic model is based on chemisorption, including the sharing or exchange of electrons between the adsorbent and the pollutant, and the valence electron forces controlling the adsorption rate are assumed for each fitting. The intraparticle diffusion model investigates the diffusion of adsorbents within adsorbent particles and reveals the effect of intraparticle diffusion on the adsorption process and the relevant equation as follows.

$$q_t = q_e(1 - e^{-k_1 t}) \quad (3)$$

$$\frac{t}{q_t} = \frac{1}{k_2 q_e^2} + \frac{1}{q_e} \quad (4)$$

$$q_t = k_{int} t^{0.5} + c \quad (5)$$

where q_e is the amount of adsorption when adsorption reaches equilibrium, mg g^{-1}; q_t is the amount of adsorption at time t, mg g^{-1}; k_1 is the adsorption rate constant of the pseudo-first-order kinetic model, min^{-1}; k_2 is the adsorption rate constant of the pseudo-second-order kinetic model, g min^{-1}; k_{int} is the internal diffusivity constant; and c is the boundary layer constant.

The results of fitting the three kinetic equations are shown in Fig. 8. The three main stages into which the adsorption process is divided can be obtained from the above results for the different reaction times, which shows that no single factor controls the adsorption steps in the process. Adsorption is generally divided into three steps: surface diffusion, diffusion

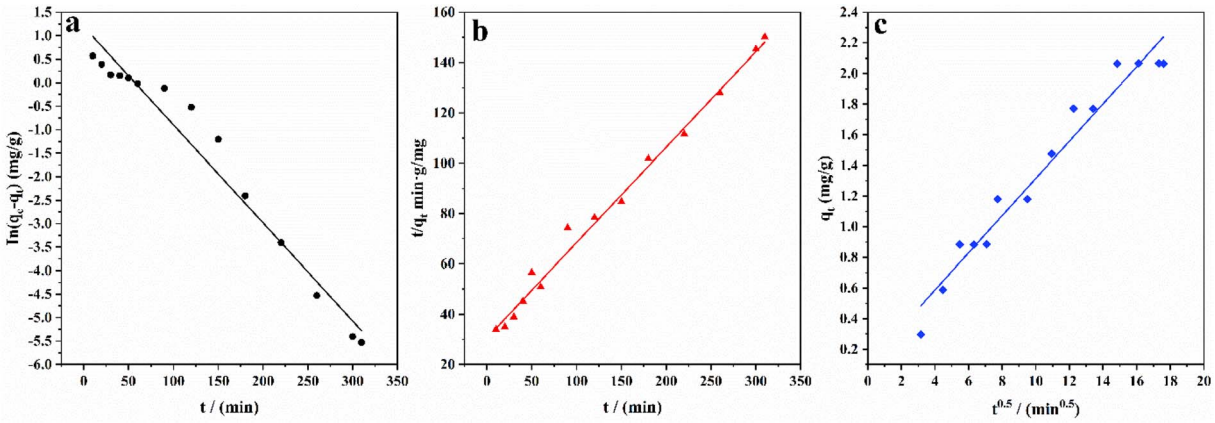

Fig. 8 Fitting curves of adsorption kinetics (a) pseudo-first-order, (b) pseudo-second-order, and (c) intraparticle diffusion. Adsorption conditions: C_0 = 6 mg L^{-1}, pH = 4, m = 1.0 g, T = 20 °C.

within the pore or particle and the interaction of the adsorbent with the adsorption site.[39–41] The results of each parameter calculation are shown in Table 2, where the determinant (R^2) of the pseudo-second-order model is 0.981, which is higher than that of the pseudo-first-order kinetic model at the same solution concentration, indicating that the adsorption of fluoride ions by ASLA/C is more consistent with the pseudo-second-order kinetic model. In addition, the q_e of the pseudo-second-order kinetic model is also more consistent with the experimentally measured sorption capacity in the results of the line plot fits.[42] Pseudo-second-order reactions are chemical reactions in which the reaction rate is proportional to the product of the concentrations of the reactants, *i.e.*, proportional to the quadratic concentration of the reactants. The pseudo-second-order kinetic model reflects the compound effect of adsorption and is based on chemisorption, suggesting that the fluoride adsorption process of ASLA/C may have involved a chemical reaction. The pseudo-second-order kinetic model fits better than the pseudo-first-order kinetic model, indicating that the adsorption of F^- by ASLA depends mainly on the amount of adsorbent in the solution and that the hydroxyl groups in fluoride and ASLA/C are adsorbed by hydrogen bonding and coordination occurs in the actual adsorption process.[43] At appropriate pH values ASLA/C can be made positively charged, so the negatively charged fluoride ions can be adsorbed. Meanwhile, the fitted curve of the intraparticle diffusion equation does not cross the origin, indicating that the adsorption process is controlled by intraparticle diffusion but is not the only rate control step.[44] Due to the high concentration gradient between the adsorbent and the adsorbed material, the initial adsorption is controlled by surface adsorption. By the time the adsorption sites on the surface are saturated, fluoride starts to enter the ASLA/C pores and is adsorbed, slowly slowing with intraparticle diffusion to reach adsorption equilibrium.[45,46] Thus, the adsorption of fluoride by ASLA is controlled by both surface diffusion and intraparticle diffusion.

Table 2 Kinetic model of fluoride sorption on the ASLA/C adsorbent

Model	Parameter	Fluoride
Pseudo-first-order	q_e/(mg g^{-1})	2.098
	k_1/(min^{-1})	0.012
	R^2	0.957
Pseudo-second-order	q_e/(mg g^{-1})	0.033
	k_2/(min^{-1})	2.638
	R^2	0.981
Intra-particle diffusion	k_{int} (mg g^{-1} $min^{-0.5}$)	0.122
	c	0.101
	R^2	0.961

3.5. Adsorption isotherms

The Langmuir, Freundlich and Temkin models were used to fit the adsorption process of ASLA/C as an adsorbent at an initial fluoride concentration of 10 mg L^{-1}. The Langmuir model assumes that adsorption is monolayer adsorption with no interaction between adsorbed molecules and that the surface adsorption energy is homogeneous. The Freundlich model suggests that the adsorbent surface is nonhomogeneous, which is dominated by multilayer adsorption, and the Temkin model incorporates adsorbent–adsorbent interactions, leading to a decrease in the heat of adsorption with decreasing coverage.[47,48] The model equation is as follows.

$$\frac{C_e}{q_e} = \frac{1}{k_L q_e^2} + \frac{1}{q_e} \quad (6)$$

$$\ln q_m = \ln K_F + \frac{1}{n} \ln C_e \quad (7)$$

$$Q_e = \left(\frac{RT}{b_T}\right) \ln(A_T C_e) \quad (8)$$

where C_e is the mass concentration at adsorption equilibrium, mg L^{-1}; k_L is the Langmuir adsorption constant, L mg^{-1}; q_e is the adsorption capacity at equilibrium, mg g^{-1}; q_m is the maximum adsorption capacity, mg g^{-1}; K_F is the Freundlich affinity coefficient, mg L^{-1}; n is the Freundlich model constant; R is the gas constant of 8.314 J (mol K)$^{-1}$; T is the absolute temperature of environmental conditions, K; b_T is the Temkin

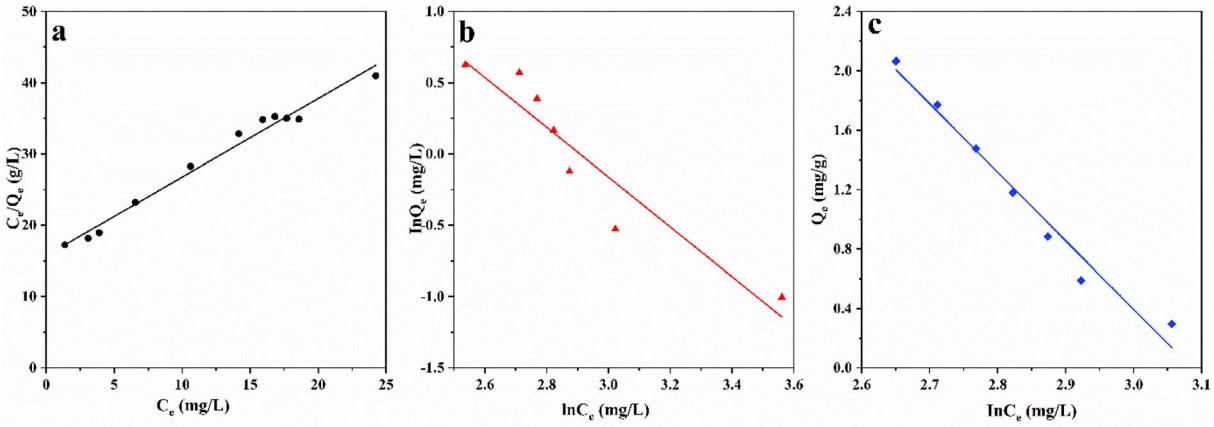

Fig. 9 Fitting curves of adsorption isotherms (a) Langmuir, (b) Freundlich, and (c) Temkin. Adsorption conditions: pH = 4, m = 1.0 g, t = 250 min, T = 20 °C.

model constant related to adsorption heat, J mol^{-1}; and A_T is the equilibrium constant related to binding energy, L mg^{-1}.

Fig. 9 shows the adsorption isotherm of ASLA/C, showing that the maximum adsorption capacity gradually increases with the increase in the initial concentration of fluoride ions. The determinant value (R^2) of the Langmuir model is 0.981 and greater than that of the Freundlich model, indicating that the Langmuir model is more suitable for this adsorption process, and the adsorption of fluoride ions by ASLA/C tends to be more of a single-molecular layer adsorption process. The weak interaction between sorbent and adsorbent (small value of parameter K_L) is a result of physical interaction. The bond energy b_T is 4.614 kJ mol^{-1} (<8 kJ mol^{-1}), as calculated by the Temkin model, so the mechanism is also influenced to some extent by physical adsorption.[49] In the physical adsorption process, the adsorbent mass is attached to the adsorbent by van der Waals interactions and this process is accompanied by a relatively low adsorption energy; thus, the process of fluoride ion adsorption by ASLA/C is mainly controlled by chemisorption and physical adsorption plays a secondary role.[50] The theoretical maximum sorption of fluorine by ASLA/C, q_{max}, was calculated by the Langmuir model to be 5.714 mg g^{-1}.

Table 3 Isotherm model of fluoride sorption on the ASLA/C adsorbent

Model	Parameter	Fluoride
Langmuir model	q_m/(mg g^{-1})	5.714
	K_L/(L mg^{-1})	0.011
	R^2	0.981
Freundlich model	K_F/(mg L^{-1})	2.031
	$1/n$	0.747
	R^2	0.873
Temkin model	A_T/(g L^{-1})	14.236
	b_T/(kJ mol^{-1})	4.614
	R^2	0.969

The mechanism of fluoride adsorption by ASLA/C as an adsorbent was investigated by studying the changes in parameters such as the Gibbs free energy (ΔG_0), enthalpy change (ΔH_0) and entropy change (ΔS_0) during the thermodynamic process of adsorption, with the following thermodynamic parameter relationships.

$$K_D = \frac{q_e}{C_e} \tag{9}$$

$$\Delta G_0 = -RT \ln K_D \tag{10}$$

$$\ln K_D = \frac{\Delta S_0}{R} - \frac{\Delta H_0}{RT} \tag{11}$$

where K_D is the adsorption diffusion coefficient; q_e is the equilibrium adsorption amount mg g^{-1}, C_e is the solution concentration in mg L^{-1} after adsorption equilibrium, K_D is calculated by eqn (9), ΔG_0 is calculated by eqn (10), and according to eqn (11), $\ln K_D$ is plotted against T^{-1}, with the intercept corresponding to ΔH_0 and the slope corresponding to ΔS_0. The results are summarized in Table 4. As Table 4 shows, $\Delta G_0 < 0$ and $\Delta H_0 > 0$, indicating that the adsorption of fluoride ions by the adsorbent is a spontaneous, heat-absorbing process, a result that is consistent with the results of the Langmuir model. ΔS_0 is determined by the constant state of the system and is independent of whether the process is reversible or not,

Table 4 Thermodynamic parameters of fluoride sorption on ASLA/C

T (K)	ΔG^0 (kJ mol^{-1})	ΔH^0 (kJ mol^{-1})	ΔS^0 (kJ mol^{-1})	E_a (kJ mol^{-1})	S^*	E (kJ mol^{-1})
283	−67.05	773.57	2.69	34 247.91	1.61×10^{-7}	90.01
293	−88.63					
303	−126.65					

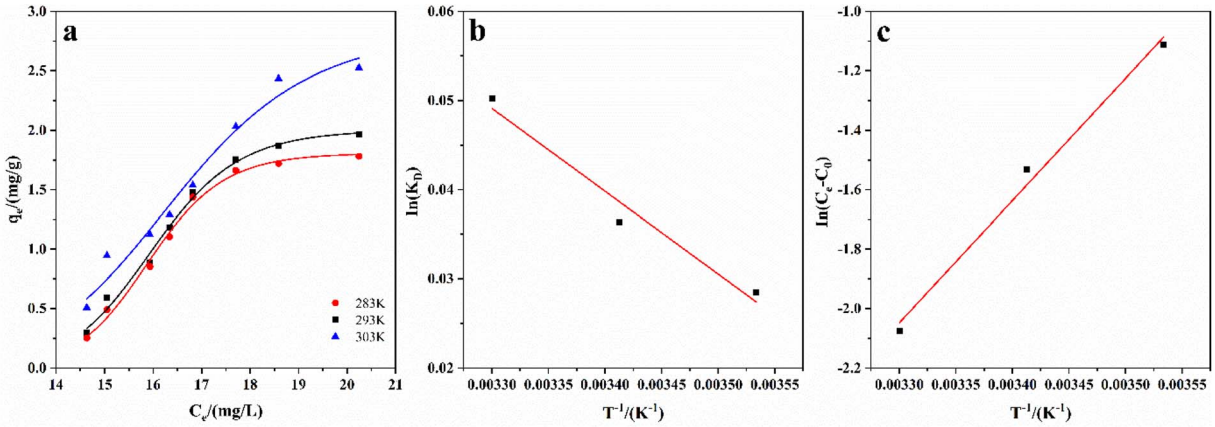

Fig. 10 (a) Adsorption isotherm fitting curve, (b) ln(K_D) in relation to T^{-1}, and (c) ln(C_e/C_0) in relation to T^{-1}. Adsorption conditions: $C_0 = 6$ mg L^{-1}, pH = 4, $m = 1.0$ g, $t = 260$ min.

and which is 93.04 kJ mol^{-1}, indicating that the adsorption process is an entropy-increasing process and the adsorption of fluoride ions is a spontaneous, heat-absorbing entropic process.[51]

The adsorption activation energy E_a is related to the Arrhenius equation as follows.

$$\ln(1-\theta) = \ln S^* + \frac{E_a}{RT} \quad (12)$$

where E_a is the activation energy of adsorption (kJ mol^{-1}), θ is the surface coverage ($\theta = 1 - C_e/C_0$) and S^* is the probability of adhesion. Plotting T^{-1} against ln(C_e/C_0) yields the straight line shown in Fig. 10, S^* and E_a are obtained from the intercept and slope of the line, and the calculation results are shown in Table 3.

The migration energy (E) represents the change in free energy as the adsorbent moves from infinity to the surface, and the type of adsorption can be determined by the migration energy. E < 8 kJ mol^{-1} (physical adsorption dominated), E > 8 kJ mol^{-1} (chemisorption dominated), and the relationship between E and each parameter is as follows.

$$E = \sqrt{-\frac{1}{2k}} \quad (13)$$

$$\ln q_e = \ln q_{max} - k\varepsilon^2 \quad (14)$$

$$\varepsilon = RT \ln\left(1 + \frac{1}{C_e}\right) \quad (15)$$

where k is a constant related to the energy of adsorption, q_{max} is the maximum adsorption capacity, q_e is the equilibrium adsorption volume and ε is the Polanyi adsorption potential. The calculated migration energy $E = 90.01$ kJ mol^{-1} indicates that the adsorption process is dominated by chemisorption, that is, when the adsorbent adsorbs fluoride ions, the randomness at the solid–liquid interface increases and the degree of disorder deepens.

3.6. Comparison of F^- adsorption capacities with those of other adsorbents

In this study, the adsorption capacity of ASLA/C for fluoride was compared with that of some other adsorbents, as shown in Table 5. The ASLA/C composite adsorbent developed in this

Table 5 Comparison between various adsorbents used for fluoride removal

Adsorbents	Removal (mg g^{-1})	Modified/raw adsorbent	Reference
Fired clay pots	1.6	Raw	52
Paper mill lime	7.37	Modified with paper mill lime mud	53
Clay composite	0.093	Thermally activated	54
Straw ash	66.23	Thermally activated	7
Electro-coagulated sludge	124.6	Thermally activated	55
Bivalve shells	0.56	Thermally activated	56
Novel clay composite	0.0856	Pyrolysis and chemically activated	57
Bentonite–smectite rich clay composite	0.6	MnO_2 modification	58
Chitosan	2.57	Raw	59
Chitosan	3.72	Rare earths modification	60
Red mud	6.15	Chitosan modification	61
Ferromagnetic nanoparticles	1.2187	Chitosan modification	62
Activated sludge lysis ash	5.714	Chitosan modification	Present study

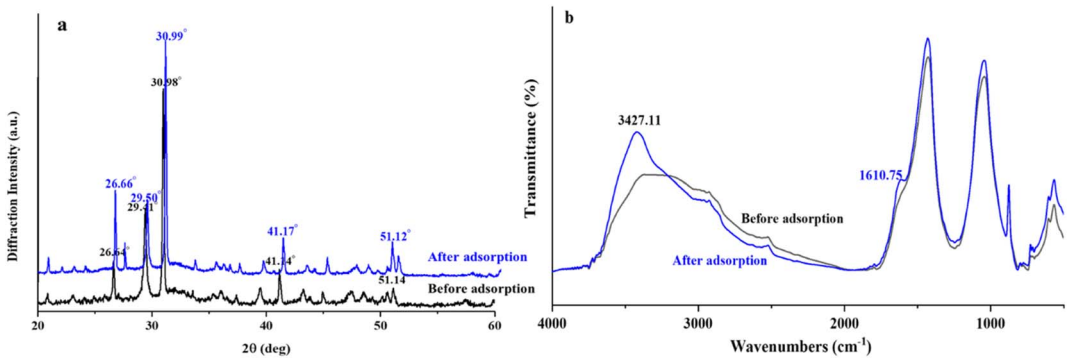

Fig. 11 Comparison of the adsorption of fluoride by ASLA/C ((a) XRD and (b) FTIR).

experiment combines chitosan with activated sludge lysis ash as a carrier, taking advantage of the high adsorption capacity of chitosan and the good mechanical properties of lysis ash, and using kaolinite as a binder to make its structure more uniform. The ASLA/C composite adsorbent was prepared, which not only retained the advantages of chitosan with a high adsorption capacity for fluoride, but also enhanced its mechanical strength. The adsorbent of this experiment is simple to prepare, does not require toxic cross-linking agent, has good stability, does not cause secondary pollution in the treated water samples, and obtains satisfactory results in several groups of experiments for fluoride removal; it can be widely collected in water plants with both economic and environmental benefits and has potential for large-scale commercial application.

3.7. Adsorption mechanism of ASLA/C

The adsorption mechanisms involved in the adsorption of fluoride by the adsorbent in this study mainly include ion exchange, electrostatic adsorption and surface complexation, accompanied by hydrogen bonding. Additionally, the dominance of a particular mechanism varies under different experimental conditions. Comparing the XRD patterns before and after adsorption of ASLA/C (Fig. 11(a)), shows that the peak shapes of the two are similar, indicating that the difference in surface structure caused by fluorine adsorption is not obvious. The shift in the main characteristic peaks representing ASLA/C, is accompanied by a slight increase in the intensity of each peak. The shift in the characteristic peaks may be attributed to the adsorption of fluoride onto the nonhomogeneous surface of ASLA *via* ion exchange, thus causing a change in its lattice.[63] In Fig. 11(b), the FTIR spectrum of the adsorbed fluoride shows a significant deepening and broadening near the 3427.11 cm^{-1} peak compared to the preadsorption spectrum, which is evidence of the formation of OH_2^+…F bonds during the adsorption process. Since –OH and F^- have similar dimensions, they can be isomerically substituted by ligand exchange; the new peak at 1610.75 cm^{-1} indicates the presence of an F…H…O bonding phase at the ASLA/C interface.

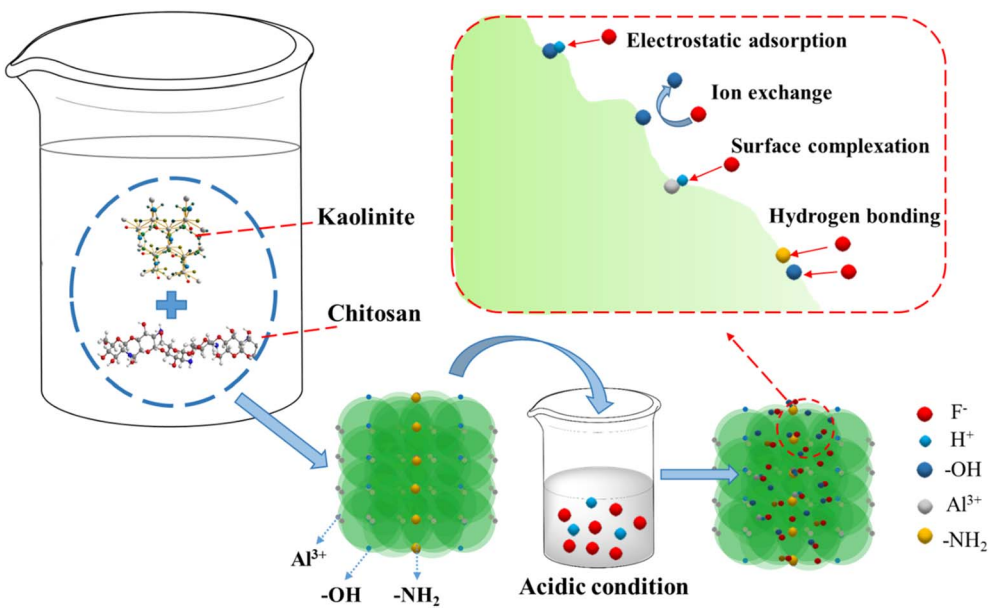

Fig. 12 Mechanism of fluoride removal by ASLA/C.

ASLA did not significantly change in terms of chemical components after chitosan modification, which may because they were compounded together by chemical bonding, and caused the formed composite adsorbent to have more pore structures formed than before modification. Chitosan contains –OH and $–NH_2$, and fluorine ions in solution can be adsorbed by exchange with –OH in the hydroxylation of the hydration reaction under the action of ion exchange. Under acidic conditions, $–NH_2$ transforms to $–NH_3^+$, which can interact with fluorine electrostatically and gravitationally; and –OH and $–NH_2$ on ASLA/C also interact with fluoride by hydrogen bonding. Meanwhile, fluorine ions can provide electrons to form strong complexes with electron-accepting high-valence metals (*e.g.*, Al and Fe). Under acidic conditions, Al^{3+} has coordinates with F^- in a stable manner and easily undergoes complexation reactions to form the stable Al–F complexes $[AlF_6]^{3+}$, $[AlF]^{2+}$, $[AlF_2]^+$, $[AlF_4]^-$, AlF_3, *etc.* (as the schematic mechanism shows in Fig. 12).

4. Conclusions

Under the present experimental conditions, the maximum adsorption capacity of fluorine using chitosan-modified activated sludge lysis ash was up to 5.714 mg g^{-1}. When the addition amount of ASLA/C was 10 g L^{-1}, the initial pH value of water was 4 and the reaction time was 250 min. The Langmuir model and the pseudo-second-order kinetic model are more suitable for the adsorption of fluorine by ASLA/C, and the adsorption of fluoride ions is a spontaneous, heat-absorbing entropic process. The increase in temperature is favourable to adsorption, and the adsorption process may have a chemical reaction. Modified ASLA/C improves the fluoride removal capacity of the material by bringing in more –OH functional groups and increasing the specific surface area of the material, and is suitable for a wide range of natural water bodies. The mechanism of fluoride removal is mainly based on three reactions: ion exchange, electrostatic adsorption and surface complexation, which are also accompanied by hydrogen bonding. Multiple removal mechanisms are better under acidic conditions with a pH of 4 to 6. Considering the wide source and low cost of activated sludge, making lysis ash for fluoride removal from wastewater has an outstanding overall cost advantage. Subsequent studies will further explore the desorption and selectivity with ASLA/C in real wastewater, and more research will be carried out on microscopic forms of material bonding and the evaluation of the full cycle of material utilisation.

Conflicts of interest

The authors declare that they have no conflicts of interest in the research described in this paper.

Acknowledgements

The authors are grateful to the Xuzhou Key Social Research and Development Program (KC18134) for providing financial support for this study. The authors would like to thank the KaiLi City Sludge Treatment Plant (Guizhou, China) for providing activated sludge lysis ash for this research.

References

1 S. V. Jadhav, E. Bringas, G. D. Yadav, V. K. Rathod, I. Ortiz and K. V. Marathe, Arsenic and fluoride contaminated groundwaters: a review of current technologies for contaminants removal, *J. Environ. Manage.*, 2015, **162**, 306–325.

2 Y. Li, N. Tsend, T. Li, H. Y. Liu, R. Q. Yang, X. K. Gai, H. P. Wang and D. S. Sheng, Microwave assisted hydrothermal preparation of rice straw hydrochars for adsorption of organics and heavy metals, *Bioresour. Technol.*, 2019, **273**, 136–143.

3 A. Jeyaseelan, M. Naushad and N. Viswanathan, Development of multivalent metal-ion-fabricated fumaric acid-based metal-organic frameworks for defluoridation of water, *J. Chem. Eng. Data*, 2020, **65**(6), 2990–3001.

4 A. Jeyaseelan, A. Kumar, N. Viswanathan and M. Naushad, Development and characterization of hydroxyapatite layered lanthanum organic frameworks by template method for defluoridation of water, *J. Colloid Interface Sci.*, 2022, **622**, 228–238.

5 Q. Mehdi, Z. Ahmad, A. Mojtaba, *et al.*, Data on cadmium removal from synthetic aqueous solution using garbage ash, *Data Brief*, 2018, **20**, 1115–1123.

6 J. Meng, M. Tao, L. Wang, X. Liu and J. Xu, Changes in heavy metal bioavailability and speciation from a Pb-Zn mining soil amended with biochars from co-pyrolysis of rice straw and swine manure, *Sci. Total Environ.*, 2018, **633**, 300–307.

7 G. Zhang, H. F. Yang, P. Fu, Z. Li and W. K. Ma, Evaluation of straw ash as a cost effective adsorbent for the removal of phosphate and fluoride from aqueous solution, *Groundw. Sustain. Dev.*, 2021, **14**, 100626.

8 T. A. Aragaw, Recycling electro-coagulated sludge from textile wastewater treatment plants as an adsorbent for the adsorptions of fluoride in an aqueous solution, *Heliyon*, 2021, **7**(6), e07281.

9 R. Mudzielwana and M. W. Gitari, Removal of fluoride from groundwater using MnO_2 bentonite-smectite rich clay soils composite, *Groundw. Sustain. Dev.*, 2021, **12**, 100623.

10 J. I. Lee, S. H. Hong, C. G. Lee and S. J. Park, Fluoride removal by thermally treated egg shells with high adsorption capacity, low cost, and easy acquisition, *Environ. Sci. Pollut. Res.*, 2021, **28**(27), 1–15.

11 R. A. Wahaab, M. Mahmoud and J. V. Lier, Toward achieving sustainable management of municipal wastewater sludge in Egypt: the current status and future prospective, *Renewable Sustainable Energy Rev.*, 2020, **127**(Jul), 109880.

12 M. Jiang, Y. Yang, T. Z. Li, Z. L. Ye and S. Q. Huang, Removal of phosphate by a novel activated sewage sludge biochar: Equilibrium, kinetic and mechanism studies, *Appl. Energy Combust. Sci.*, 2022, **9**, 100056.

13 J. H. Wang, R. H. Cao, D. He and A. Saleem, Facile preparation of polyethyleneimine modified activated sludge-based

adsorbent for hexavalent chromium removal from aqueous solution, *Sep. Sci. Technol.*, 2020, **56**(3), 498–506.

14 C. I. Akor, A. I. Osman, C. Farrell, C. S. McCallum and W. John Doran, Thermokinetic study of residual solid digestate from anaerobic digestion, *Chem. Eng. J.*, 2020, **406**, 127039.

15 A. I. Osman, A. M. Elgarahy, N. Mehta, A. H. Al-Muhtaseb, A. S. Al-Fatesh and D. W. Rooney, Facile Synthesis and Life Cycle Assessment of Highly Active Magnetic Sorbent Composite Derived from Mixed Plastic and Biomass Waste for Water Remediation, *ACS Sustainable Chem. Eng.*, 2022, **10**, 12433–12447.

16 X. D. Li, Y. W. Guo, J. Y. Cai and W. Bao, Experimental study on the treatment of acid mine drainage containing heavy metals with domestic waste pyrolysis ash, *Water Sci. Technol.*, 2022, **85**(11), 3225–3239.

17 A. I. Osman, E. O'Connor, G. McSpadden, J. K. Abu-Dahrieh, C. Farrell, A. H. Al-Muhtaseb, J. Harrison and D. W. Rooney, Upcycling brewer's spent grain waste into activated carbon and carbon nanotubes for energy and other applications *via* two-stage activation, *J. Chem. Technol. Biotechnol.*, 2020, **95**, 183–195.

18 F. F. Xiao, J. H. Cheng, W. Cao, C. Yang, J. F. Chen and Z. F. Luo, Removal of heavy metals from aqueous solution using chitosan-combined magnetic biochars, *J. Colloid Interface Sci.*, 2019, **540**, 579–584.

19 C. F. Zheng, H. L. Zheng, Y. J. Sun, B. C. Xu, Y. L. Wang, X. Y. Zheng and Y. J. Wang, Simultaneous adsorption and reduction of hexavalent chromium on the poly (4-vinyl pyridine) decorated magnetic chitosan biopolymer in aqueous solution, *Bioresour. Technol.*, 2019, **293**, 122038.

20 S. J. Wu, M. Y. Li, L. Xin, H. M. Long and X. P. Gao, Efficient removal of Cr(VI) by triethylenetetramine modified sodium alginate/carbonized chitosan composite *via* adsorption and photocatalytic reduction, *J. Mol. Liq.*, 2022, **366**, 120160.

21 X. Q. Liu, Y. Y. Zhang, Y. Liu and T. Zhang, Magnetic red mud/chitosan based bionanocomposites for adsorption of Cr(VI) from aqueous solutions: synthesis, characterization and adsorption kinetics, *Polym. Bull.*, 2022, **6**, 1–20.

22 A. I. Osman, C. Farrell, A. H. Al-Muhtaseb, J. Harrison and D. W. Rooney, The production and application of carbon nanomaterials from high alkali silicate herbaceous biomass, *Sci. Rep.*, 2021, **10**, 2563.

23 L. C. Kong, Y. T. Zheng, Z. Pang, X. H. Huang, M. Li, R. C. Yang, N. Li, J. Zhang and W. Zuo, Synchronous phosphate and fluoride removal from water by 3d rice-like lanthanum-doped La@MgAl nanocomposites, *Chem. Eng. J.*, 2019, **371**, 893–902.

24 K. K. Alau, C. E. Gimba, B. E. Agbaji and S. E. Abechi, The activated carbon were produced from neem (Azadirachta Indica) husk and seed and activated with ZnCl2 and H3PO4. The prepared adsorbents were used, *Appl. Sci. Res.*, 2010, **2**, 451–455.

25 S. Natalia, Surgutskaia, Antonio Di Martino, Jiri Zednik, Kadir Ozaltin, Lenka Lovecká, Eva Domincová Bergerová, Dušan Kimmer, Jan Svoboda, Vladimir Sedlarik. Efficient Cu^{2+}, Pb^{2+} and Ni^{2+} ion removal from wastewater using electrospun DTPA-modified chitosan/polyethylene oxide nanofibers, *Sep. Purif. Technol.*, 2020, **247**, 116914.

26 M. Q. Jiang, X. Y. Jin, X. Q. Lu and Z. L. Chen, Adsorption of Pb(II), Cd(II), Ni(II) and Cu(II) onto natural kaolinite clay, *Desalination*, 2010, **252**, 33–39.

27 Y. F. Li, X. N. Zhang, C. Yan and H. Y. Li, Study on the effect of Al-modified zeolite in the treating of fluorinated water and its influencing factors, *International Symposium on Water Resource & Environmental Protection*, 2011, pp. 2061–2064.

28 A. Jeyaseelan, A. Kumar, M. Naushad and N. Viswanathan, Fabrication of hydroxyapatite embedded cerium-organic frameworks for fluoride capture from water, *J. Mol. Liq.*, 2022, **354**, 118830.

29 M. Islam and R. Patel, Thermal activation of basic oxygen furnace slag and evaluation of its fluoride removal efficiency, *Chem. Eng. J.*, 2011, **169**, 68–77.

30 S. V. Mohan, N. C. Rao and J. Karthikeyan, Adsorptive removal of direct azo dye from aqueous phase onto coal based sorbents: a kinetic and mechanistic study, *J. Hazard. Mater.*, 2002, **90**, 189–204.

31 M. M. Damtie, C. W. Yun, B. Kim, R. H. Hailemariam and J. S. Choi, Removal of fluoride in membrane-based water and wastewater treatment technologies: performance review, *J. Environ. Manage.*, 2019, **251**, 109524.

32 S. Singh, A. Khare and S. Chaudhari, Enhanced fluoride removal from drinking water using non-calcined synthetic hydroxyapatite, *J. Environ. Chem. Eng.*, 2020, **8**, 103704.

33 S. Gogoi, S. K. Nath, S. Bordoloi and R. K. Dutta, Fluoride removal from groundwater by limestone treatment in presence of phosphoric acid, *J. Environ. Manage.*, 2015, **152**, 132–139.

34 J. F. Zhang, T. E. Brutus, J. M. Cheng and X. G. Meng, Fluoride removal by Al, Ti, and Fe hydroxides and coexisting ion effect, *J. Environ. Sci.*, 2017, 190–195.

35 Z. Chen, Y. Liu, L. Mao, L. Gong, W. Sun and F. Li, Effect of cation doping on the structure of hydroxyapatite and the mechanism of defluoridation, *Ceram. Int.*, 2018, **44**, 6002–6009.

36 T. Zhang, X. Jin, G. Owens and Z. Chen, Remediation of malachite green in wastewater by zif-8@Fe/Ni nanoparticles based on adsorption and reduction, *J. Colloid Interface Sci.*, 2021, **594**, 398–408.

37 A. Byungryul, Applicability of adsorption kinetic model for cation/anion for chitosan hydrogel bead, *J. Korean Soc. Water Wastewater*, 2019, **33**, 205–213.

38 E. N. Ranasinghe and B. M. W. P. K. Amarasinghe, Single and Binary Adsorption of Heavy Metal Ions from Aqueous Solutions Using Coirpith as the Adsorbent, *Int. Conf. Sustainable Built Environ.*, 2020, **44**, 75–90.

39 J. L. Wang and X. Guo, Adsorption kinetic models: Physical meanings, applications, and solving methods, *J. Hazard. Mater.*, 2020, **390**, 122156.

40 Y. Wang, X. Dai, Y. Zhan, X. Ding and X. Wang, In situ growth of ZIF-8 nanoparticles on chitosan to form the hybrid nanocomposites for high-efficiency removal of congo red, *Int. J. Biol. Macromol.*, 2019, **137**, 77–86.

41 Q. Qin, M. Li, P. Lan, Y. Liao, S. Sun and H. Liu, Novel $CaCO_3$/chitin aerogel: synthesis and adsorption performance toward congo red in aqueous solutions, *Int. J. Biol. Macromol.*, 2021, **181**, 786–792.

42 J. Dai, X. Xiao, S. X. Duan, J. Liu, J. He, J. D. Lei and L. Y. Wang, Synthesis of novel microporous nanocomposites of ZIF-8 on multiwalled carbon nanotubes for adsorptive removing benzoic acid from water, *Chem. Eng. J.*, 2018, **331**, 64–74.

43 C. Aoopngan, J. Nonkumwong, S. Phumying, W. Promjantuek and L. Srisombat, Amine-functionalized and hydroxyl-functionalized magnesium ferrite nanoparticles for congo red adsorption, *ACS Appl. Nano Mater.*, 2019, **2**, 5329–5341.

44 Z. Salahshoor and A. Shahbazi, Modeling and optimization of cationic dye adsorption onto modified sba-15 by application of response surface methodology, *Desalin. Water Treat.*, 2016, **57**, 13615–13631.

45 H. Qian, Y. L. Lin, B. Xu, L. P. Wang, Z. C. Gao and N. Y. Gao, Adsorption of haloforms onto gacs: effects of adsorbent properties and adsorption mechanisms, *Chem. Eng. J.*, 2018, **349**, 849–859.

46 E. Zuaa, B. Ly, W. C. Jin, E. Ddga, E. Fia and E. Qla, Neodymium embedded ordered mesoporous carbon (omc) for enhanced adsorption of sunset yellow: characterizations, adsorption study and adsorption mechanism, *Chem. Eng. J.*, 2019, **359**, 814–826.

47 E. C. Nnadozie and P. A. Ajibade, Data for experimental and calculated values of the adsorption of Pb(II) and Cr(VI) on aptes functionalized magnetite biochar using Langmuir, Freundlich and Temkin equations, *Data Brief*, 2020, **32**, 106292.

48 C. S. T. Araújo, I. L. S. Almeida, H. C. Rezende, S. M. L. O. Marcionilio, J. J. L. Léon and T. N. de Matosd, Elucidation of mechanism involved in adsorption of Pb(II) onto lobeira fruit (*Solanum lycocarpum*) using Langmuir, Freudlich and Temkin isotherms, *Microchem. J.*, 2018, **137**, 348–354.

49 B. Mi, J. Wang, H. Xiang, F. Liang and B. Fei, Nitrogen self-doped activated carbons derived from bamboo shoots as adsorbent for methylene blue adsorption, *Molecules*, 2019, **24**, 3012.

50 M. Hermassi, C. Valderrama, N. Moreno, O. Font, X. Querol, N. H. Batis and J. L. Cortina, Fly ash as reactive sorbent for phosphate removal from treated waste water as a potential slow release fertilizer, *J. Environ. Chem. Eng.*, 2017, **5**, 160–169.

51 F. A. Ngwabebhoh, M. Gazi and A. A. Oladipo, Adsorptive removal of multi-azo dye from aqueous phase using a semi-ipn superabsorbent chitosan-starch hydrogel, *Chem. Eng. Res. Des.*, 2016, **112**, 274–288.

52 G. P. Kofa, V. H. Gomdje, C. Telegang and K. S. Ndi, Removal of fluoride from water by adsorption onto fired clay pots: kinetics and equilibrium studies, *J. Appl. Chem.*, 2017, 1–7, DOI: **10.1155/2017/6254683**.

53 C. W. Ye, B. W. Yan, X. Ji, B. Liao, R. Gong, X. J. Pei and G. Liu, Adsorption of fluoride from aqueous solution by fly ash cenospheres modified with paper mill lime mud: experimental and modeling, *Ecotoxicol. Environ. Saf.*, 2019, **180**, 366–373.

54 L. D. Gidi, E. Z. Amare, H. Murthy and B. Abebe, Application of novel clay composite adsorbent for fluoride removal, *Mater. Sci. Res. India*, 2019, **16**, 164–173.

55 A. E. Yilmaz, B. A. Fil, S. Bayar and Z. K. Karaka, A new adsorbent for fluoride removal: the utilization of sludge waste from electrocoagulation as adsorbent, *Global NEST J.*, 2015, **17**, 186–197.

56 S. Y. N'Zébo, H. B. Bi Gouessé, S. Aw, L. Reinert and K. Adouby, Bivalve shells (Corbula trigona) as a new adsorbent for the defluoridation of groundwater by adsorption-precipitation, *J. Environ. Sci. Health, Part A: Toxic/Hazard. Subst. Environ. Eng.*, 2021, **56**, 1–11.

57 A. Balouch, M. Kolachi, F. N. Talpur, H. Khan and M. I. Bhanger, Sorption kinetics, isotherm and thermodynamic modeling of defluoridation of ground water using natural adsorbents, *Am. J. Anal. Chem.*, 2013, **4**(5), 221–228.

58 R. Mudzielwana and M. W. Gitari, Removal of fluoride from groundwater using mno2 bentonite-smectite rich clay soils composite, *Groundw. Sustain. Dev.*, 2021, **12**, 100623.

59 H. Akbari, S. Jorfi, A. H. Mahvi, M. Yousefi and D. Balarak, Adsorption of fluoride on chitosan in aqueous solutions: determination of adsorption kinetics, *Fluoride*, 2021, **51**, 319–327.

60 P. Liang, Y. Zhang, D. F. Wang, Y. Xu and L. Luo, Preparation of mixed rare earths modified chitosan for fluoride adsorption, *J. Rare Earths*, 2013, **31**, 817–822.

61 X. Liu, Y. Zhang, Y. Liu and T. Zhang, Magnetic red mud/chitosan based bionanocomposites for adsorption of Cr(VI) from aqueous solutions: synthesis, characterization and adsorption kinetics, *Polym. Bull.*, 2022, DOI: **10.1007/s00289-022-04137-x**.

62 E. Mohammadi, H. Daraei, R. Ghanbari, S. D. Athar, Y. Zandsalimi, A. Ziaee and A. M. bK. Yetilmezsoy, Synthesis of carboxylated chitosan modified with ferromagnetic nanoparticles for adsorptive removal of Fluoride, Nitrate, and Phosphate anions from aqueous solutions, *J. Mol. Liq.*, 2019, **273**, 116–124.

63 B. Nayak, A. Samant, R. Patel and P. K. Misra, Comprehensive understanding of the kinetics and mechanism of fluoride removal over a potent nanocrystalline hydroxyapatite surface, *ACS Omega*, 2017, **2**, 8118–8128.